Annex B

ATMOSPHERIC TRANSPORT MODULE VERIFICATION

The atmospheric transport scheme of the models developed is described in Chapter 4. This annex contains description of some numerical experiments verifying the transport module consistency.

B.1 Testing of the advection scheme

Horizontal advection

To examine the consistency of the constructed advection scheme the classical Smolarkiewicz numerical experiments [*Smolarkiewicz*, 1982] have been performed. In the first experiment initial distribution of ψ is transported in the uniform rotational flow. In the second one transformation of the initial distribution in the strong deformational flow is considered. In both numerical experiments cone-shaped initial distribution has been determined with ψ=110 at the top and ψ=10 at the bottom of the cone (arbitrary units).

The objective of the rotational flow experiment is to examine the model ability to simulate a pollutant horizontal advective transport and to evaluate artificial diffusion of the numerical scheme. The wind field of the rotational flow is shown in Figure B.1 as well as the initial cone shaped distribution. The axis of the rotational flow is sloped down from the Earth axis with the angle 30° and the center of the initial distribution is located at the latitude 20°N. Since the flow is non-divergent the uniform distribution should remain uniform, while the cone-shaped one theoretically should be transported as a solid body. However, in reality the cone is smoothed down due to the artificial diffusion.

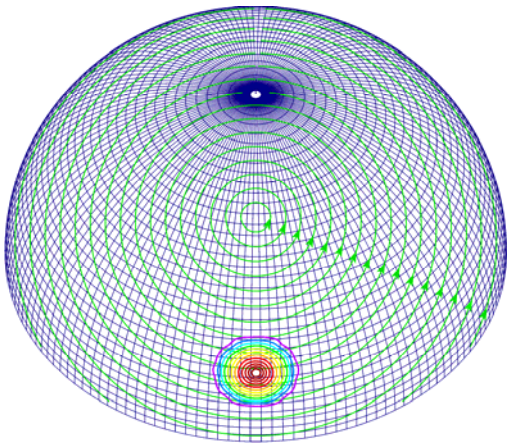

Figure B.1. *Conditions of the rotational flow numerical experiment: Wind streamlines and the initial cone-shaped distribution. Concentric circles denote isolines of ψ value with step $\Delta\psi$ = 8 (arbitrary units)*

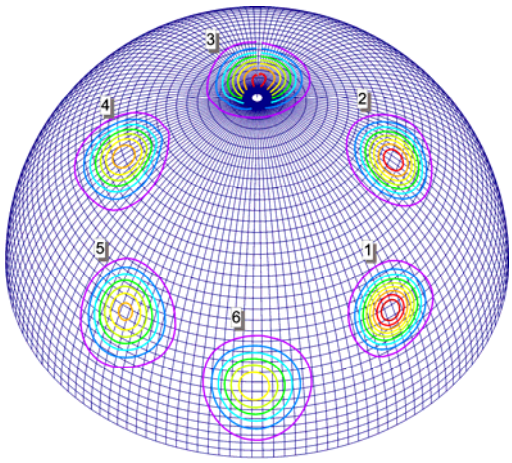

Figure B.2. *Results of the rotational flow numerical experiment. Concentric circles denote isolines of ψ value with step $\Delta\psi$ = 8 (arbitrary units): 1 – after 1/6 of the full revolution; 2 – 1/3; 3 – 1/2; 4 – 2/3; 5 – 5/6; 6 – after the full revolution*

Results of the test are presented in Figure B.2. The numbered sets of concentric circles show the cone location and shape at different moments of the revolution with time step Δt=1/6 of the whole revolution period. As seen from the figure the cone only slightly changes its shape due to numerical dispersion and artificial diffusion after the whole revolution. It has become lower (about 60% of the original height) and its circular shape has been somewhat disturbed. Thus, the advection scheme does not produce considerable distortions and has comparatively low artificial diffusion.

The objective of the deformational flow experiment is to examine the model stability in strong deformational flows and evaluate possible time-splitting error [*Bott*, 1993; *Easter*, 1993; *Clappier*, 1998]. The velocity field and the initial cone-shaped distribution for the deformational flow experiment are presented in Figure B.3 in spherical coordinates. Zonal and meridional components of the wind are determined by the following formulas:

$$V_\lambda = 4\sin(4\lambda)\sin(4\varphi - \pi/2),$$

$$V_\varphi \cos\varphi = 4\cos(4\lambda)\cos(4\varphi - \pi/2).$$

As it is seen from the figure the wind field is built up from sets of symmetrical vortices. Since the flow is non-divergent again a uniform distribution should remain uniform except zones where mass from the initial cone incoming. But anyway values of ψ should remain limited at any point of the domain.

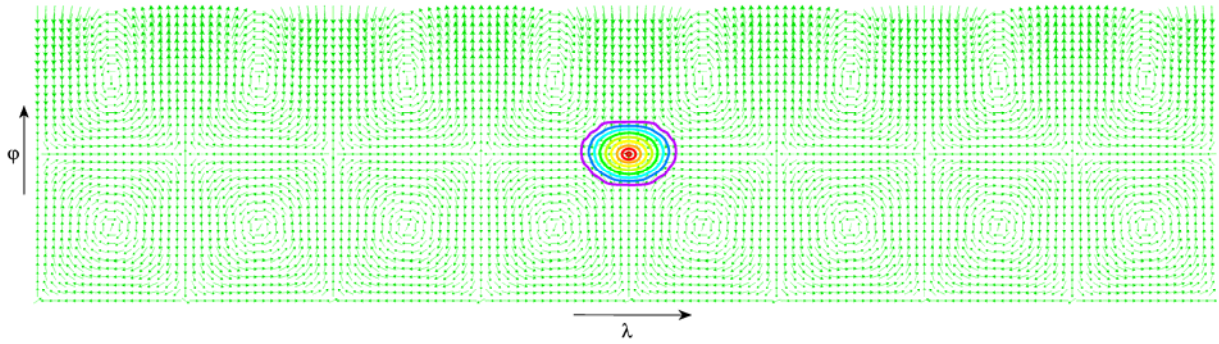

Figure B.3. *Conditions of the deformational flow numerical experiment: Wind velocity vectors and the initial cone-shaped distribution. Concentric circles denote isolines of ψ value with step $\Delta\psi$ = 10 (arbitrary units)*

Results of the experiment are presented in Figure B.4. Figure B.4.a shows the initial cone-shaped distribution in the spherical coordinates. Figures B.4.b–e illustrate transformation of the distribution in the deformation flow and correspond to different time moments (or different numbers of iterations). As one can see the mass is coming along the boundaries of the vortices and is penetrating to the neighboring ones. The main difference from the original deformational flow experiment [*Smolarkiewicz*, 1982] is sharing of the mass between the remote vortices through the pole (see Fig.B.4.d). This is peculiar feature of the spherical geometry. The maximum value of ψ distribution decreases in time, that is the model is stable to the deformational flow. Besides, there is no observable time-splitting error.

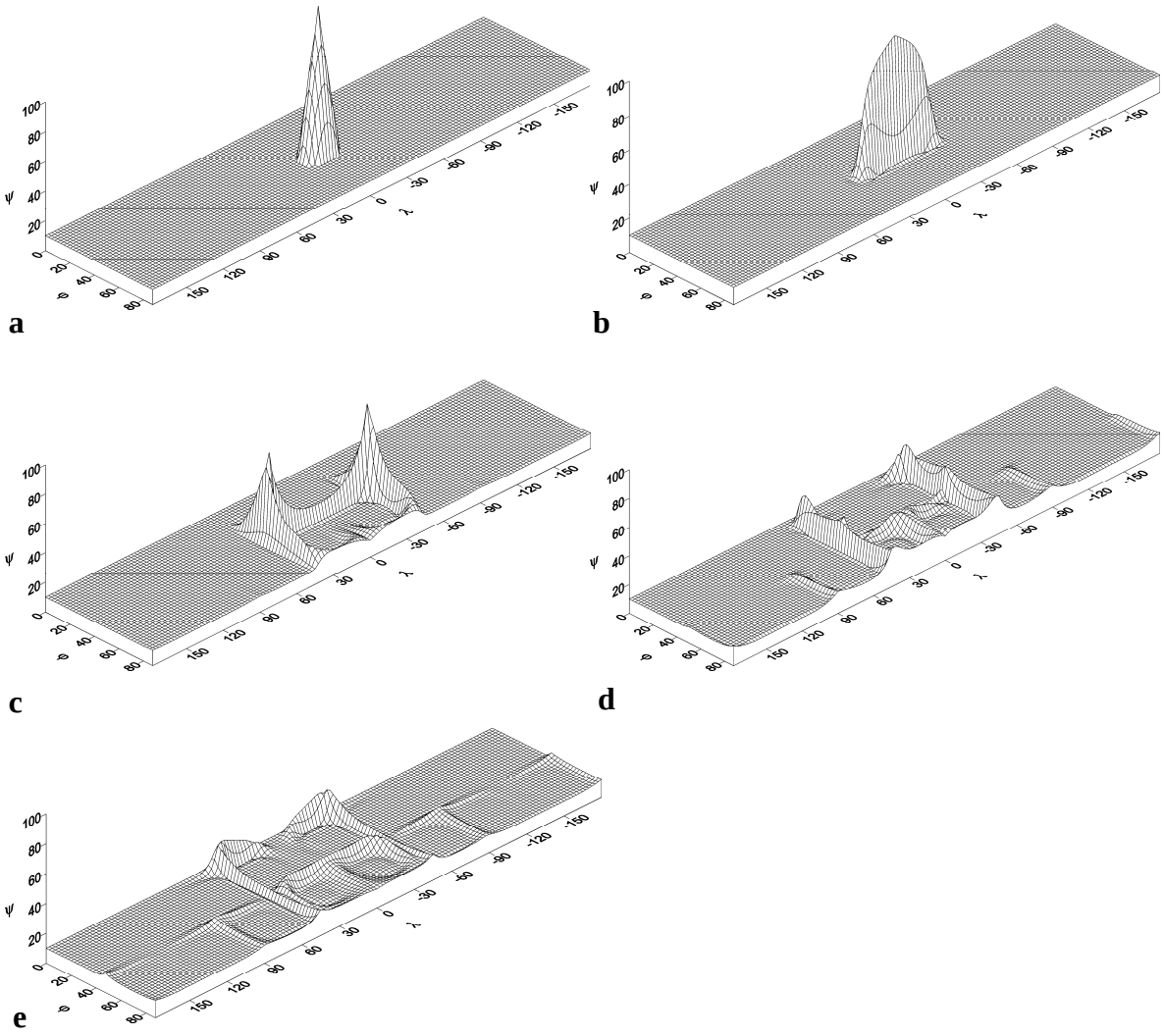

Figure B.4. *Results of the deformational flow numerical experiment ψ distribution: (a) – initial; (b) – after 130 iterations; (c) – 390 iterations; (d) – 650 iterations; (e) – 810 iterations*

Vertical advection

To examine the vertical advective transport in combination with the horizontal one a number of numerical experiments have been performed. One of them is presented below. Two-dimensional advective transport is considered. Conditions and results of the experiment are shown in Figure B.5. The real orography corresponding to 100°E longitude is utilized as a underlying surface. To simulate straight-line transport of the initial distribution in the terrain-following coordinates the uniform wind field has been determined along the horizon (see Fig.B.5.a). For this purpose we had to apply

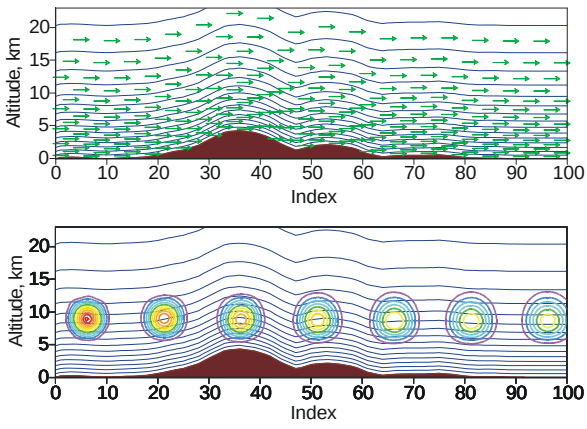

Figure B.5. *Wind field (a) and results (b) of the numerical experiment for the vertical advection*

unrealistic “transparent” boundary conditions at the surface: The wind can freely flow in and out through the surface. The main objective of the experiment is to examine the model ability to adequately simulate the advective transport in the atmosphere without influence of the curvilinear sigma coordinate. The cone-shaped initial distribution is determined in the left side of the domain (see Fig.B.5.b) and moves to the right. As one can see from the figure the cone is transported along straight line, and somewhat smoothing of the initial shape is observed due to the artificial diffusion. The originally circular shape is slightly disturbed because of the non-uniform grid.

B.2 Verification of the atmospheric transport module

The atmospheric module requires to be verified against some reliable results of other models or measurements. First of all we compared modeling results obtained by the hemispheric model with those by regional MSCE-HM model of heavy metal atmospheric transport. The MSCE-HM model has been developed and employed in operational regime for the last several years. It has been verified in a number of intercomparison campaigns with other regional models [*Sofiev et al.*, 1996; *Gusev et al.*, 2000; *Ryaboshapko et al.*, 2001] and has been qualified by means of sensitivity and uncertainty studies [*Travnikov*, 2000]. Thus its results can be considered as quite reliable within European region. In the other verification procedure the hemispheric model results were compared with measurement data available within the EMEP monitoring network. In both cases lead airborne transport was considered.

Comparison with regional MSCE-HM model

The regional MSCE-HM model is a three-dimensional Eulerian-type model operating within the EMEP domain (see Fig.B.6). The model grid covers whole Europe, the Mediterranean Sea, and part of the Atlantic Ocean with spatial resolution 50 km × 50 km. In the vertical it consists of 5 atmospheric layers up to approximately 4 km. Detailed description of the model can be found in [*Ryaboshapko et al.*, 1999].

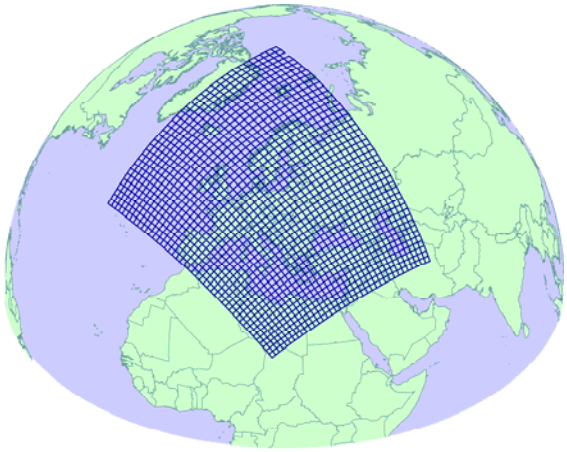

Figure B.6. *Computation domain of the regional MSCE-HM model (EMEP domain)*

Conditions of the comparison are summarized in Table B.1. Both models were employed to calculate the long-range transport and deposition of antropogenic lead in 1990. Each model used its own computation domain and spatial resolution. In both cases we used meteorological data for 1990. The MSCE-HM model utilized official anthropogenic emission data from the EMEP inventory while the hemispheric model operated with the GEIA Global Lead Emission Inventory for 1989 [*Pacyna et al.*, 1995]. Only European emission sources were considered from the whole hemispheric field. Since the official EMEP data considerably differ from the GEIA inventory, we had to reduce the latter by multiplying the emission field by a correction factor (~0.6) to equalize the total emissions from Europe in both cases. The spatial fields of lead anthropogenic emission density for regional MSCE-HM and hemispheric models are presented in Figures B.7 and B.8 respectively.

Table B.1. *Conditions of the hemispheric and regional MSCE-HM models comparison study*

Characteristics	Hemispheric model	MSCE-HM model
Objective	Lead long-range transport and deposition in 1990	
Computation domain	Northern Hemisphere	EMEP domain
Spatial resolution	2.5° × 2.5°	50 km × 50 km
Meteorological data	for 1990	for 1990
Emission data	Reduced GEIA inventory for 1989	Official data from the EMEP inventory for 1990

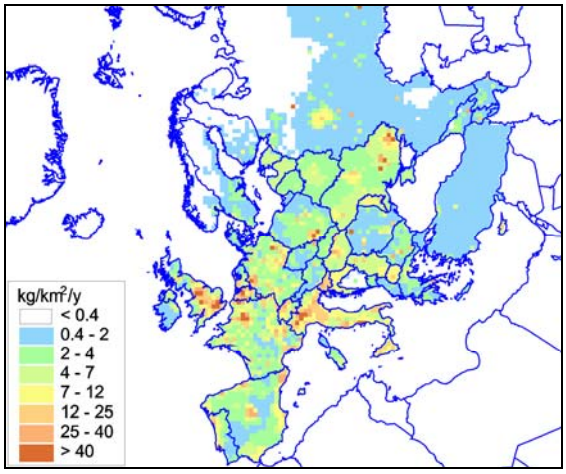

Figure B.7. *Lead anthropogenic emission density in 1990 (official data from the EMEP inventory)*

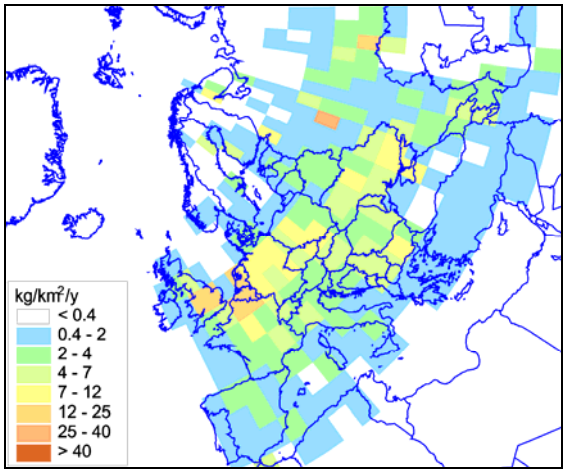

Figure B.8. *Lead anthropogenic emission density in 1989 (reduced GEIA Inventory)*

As seen from the figures, considerably lower resolution of the hemispheric model leads to rougher distribution of the anthropogenic emissions smoothing all emission peaks (Fig. B.8). Besides, the emission fields have some spatial distinctions. First of all one has to mention significantly higher emission levels for the regional model (Fig. B.7) in Northern Italy and in Spain.

Results of the model comparison are presented in Figures B.9–B.14. Figures B.9 and B.10 show spatial distributions of mean annual lead concentration in surface air obtained by the MSCE-HM and hemispheric models respectively.

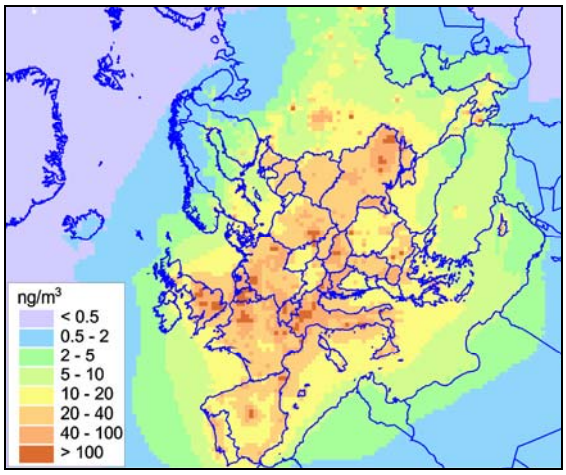

Figure B.9. *Spatial distribution of mean annual lead concentration in the surface air obtained by the* ***regional MSCE-HM model***

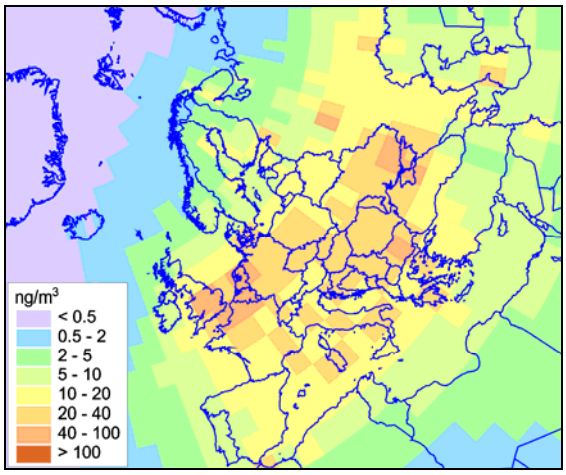

Figure B.10. *Spatial distribution of mean annual lead concentration in the surface air obtained by the* ***hemispheric model***

Here one should take into account that the models have quite different advection schemes, spatial resolutions, and utilize different emission data. Nevertheless, the spatial distribution fields in both cases look quite similar. The regions with the highest lead concentrations coincide as a whole, except several regions (e.g. Northern Italy, Spain etc.), where the hemispheric model produce considerably lower values. The reason for the distinction is different emission fields for the regional and hemispheric models as it was mentioned above (compare Fig.B.6 and B.7). The models produce very close background lead concentrations in air far from industrial regions (e.g. the Atlantic Ocean and the Arctic) characterizing long-range lead transport. It is natural that the concentration field of the hemispheric model is smoother (without significant peaks) than that of the regional one due to lower spatial resolution. Besides, the hemispheric model predicts more considerable lead transport outside the domain eastward and south-eastward. A similar situation is for the spatial distributions of total annual lead deposition (compare Fig. B.11 and B.12).

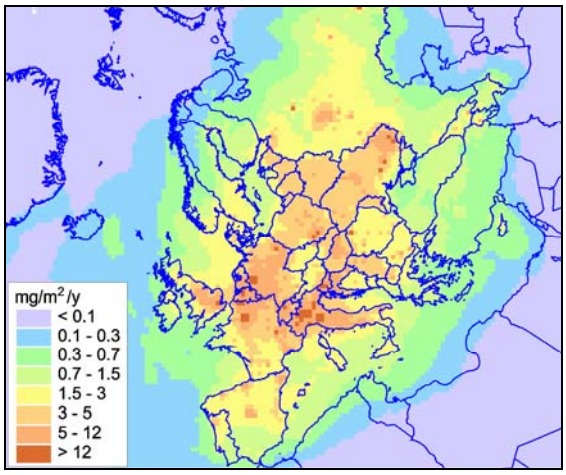

Figure B.11. *Spatial distribution of total annual lead deposition obtained by the* ***regional MSCE-HM model***

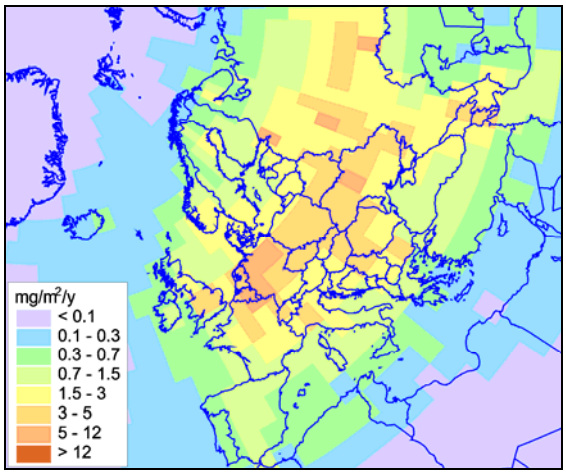

Figure B.12. *Spatial distribution of total annual lead deposition obtained by the* ***hemispheric model***

Quantitative comparison of the concentration and deposition fields obtained by the regional and hemispheric models has been performed by means of regression analysis and is presented in Figures B.13 and B.14. We compared values of mean annual lead concentration in air (Fig. B.13) and total annual lead deposition (Fig. B.14) obtained by both models at grid points of the EMEP domain. To avoid excessive overloading of the figures we present only one sixth of all the grid cells uniformly distributed over the domain. As seen from the figures the slopes of the regression line are quite close to unity (solid blue line) and correlation coefficients (R) are higher than 0.7 in both cases. The significant overshoots of the regional model results can be explained by considerably higher resolution and correspond to points with the highest emission. As a whole the most points are within a “factor of two” limits (dashed blue lines).

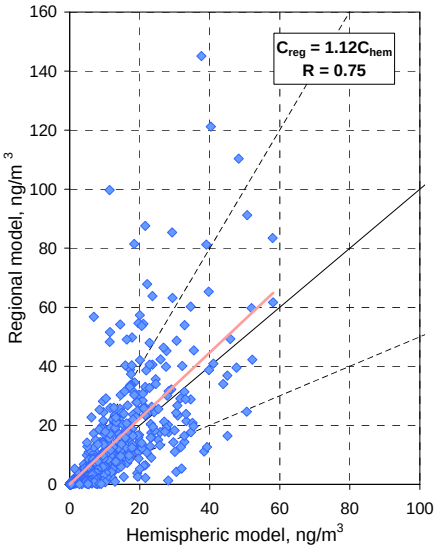

Figure B.13. *Comparison of the mean annual lead concentration fields obtained by the regional MSCE-HM and hemispheric models. Equation $C_{reg} = AC_{hem}$ describes the regression line with the slope A; R is the correlation coefficient*

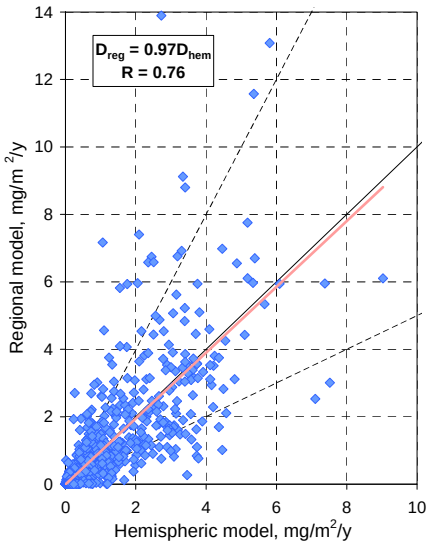

Figure B.14. *Comparison of the annual total lead deposition fields obtained by the regional MSCE-HM and hemispheric models. Equation $D_{reg}=AD_{hem}$ describes the regression line with the slope A; R is the correlation coefficient*

Comparison with measurements

In order to verify the hemispheric model consistency we also compared the modeling results with the available measurements. The original (not reduced) emission data for lead in 1989 from the GEIA Inventory [*Pacyna et al.*, 1995] were used for the modeling. The measurement data for lead in 1989 were taken from the EMEP monitoring network [*Berg et al.,* 1996]. The comparison of the observed and modeled mean annual lead concentrations in the surface air and annual wet deposition fluxes are presented in Figures B.15 and B.16 respectively. As seen from the figures the modeling results are in a satisfactory agreement with observations in both cases. The model overestimates the observed air concentrations at the most monitoring stations (see Fig. B.15). As one can see from the regression analysis (Figs. B.15.b and B.16.b) the discrepancy of the modeling results and measurements mostly does not exceed a factor of two.

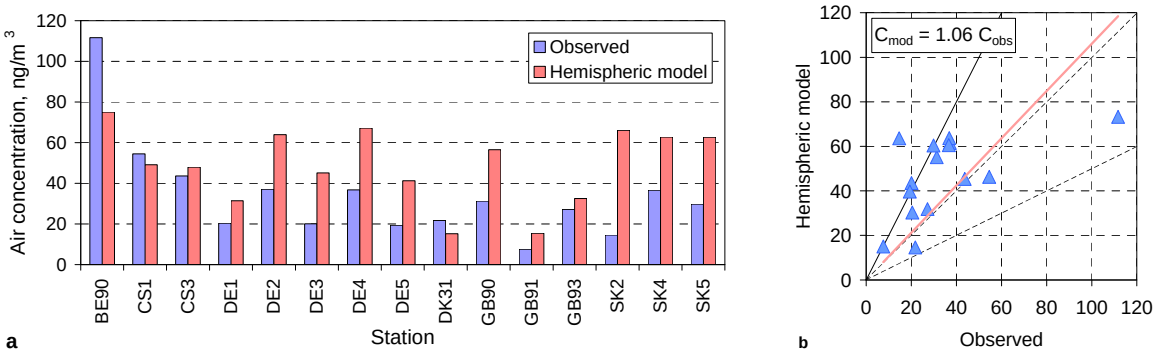

Figure B.15. *Observed and modeled mean annual lead concentrations in the surface air, ng/m^3*

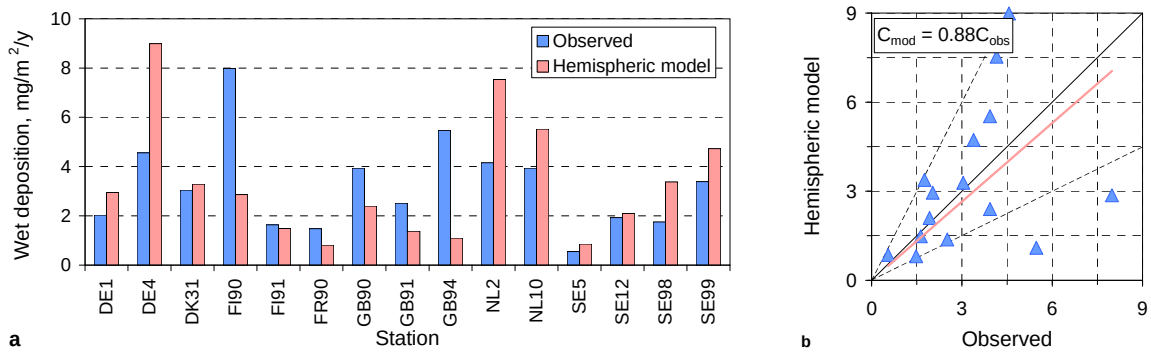

Figure B.16. *Observed and modeled annual wet deposition fluxes, mg/m^2/y*

References

Berg T., A.-G. Hjellbrekke and J.E. Skjelmoen [1996]: Heavy metals and POPs within the ECE region. EMEP/CCC-Report 8/96. Norwegian Institute for Air Research.

Bott A. [1993] The monotone area-preserving flux-form advection algorithm: Reducing the time-splitting error in two-dimensional flow fields. *Monthly Weather Review,* v.121, pp.2637-2641.

Clappier A. [1998] A correction method for use in multidimensional time-splitting advection algorithms: Application to two- and three-dimensional transport. *Monthly Weather Review,* v.126, pp. 232–242.

Easter R. C. [1993] Two modified versions of Bott's positive-definite numerical advection scheme. *Monthly Weather Review,* v.121, pp.297-304.

Gusev A., Ilyin I., Petersen G., van Pul A., Syrakov D., and Pekar M. [2000] Long-range transport model intercomparison studies. EMEP/MSC-E Technical note 2/2000, Meteorological Synthesizing Centre – East, Moscow, Russia.

Pacyna J. M., Scholtz M. T., and Li Y.-F. [1995] Global Budgets of Trace Metal Sources, *Environmental Reviews*, v.3, pp.145-159.

Ryaboshapko A., Ilyin I., Gusev A., Afinogenova O., Berg T. and Hjellbrekke A.-G. [1999] Monitoring and modelling of lead, cadmium and mercury transboundary transport in the atmosphere of Europe. Joint report of EMEP centres: MSC-E and CCC, EMEP Report 3/99, Meteorological Synthesizing Centre – East, Moscow, Russia

Ryaboshapko A., Ilyin I., Bullock R., Ebinghaus R., Lohman K., Munthe J., Petersen G., Segneur C., Wangberg I. [2001] Intercomparison study of numerical models for long-range atmospheric transport of mercury. Stage I: Comparison of chemical modules for mercury transformations in a cloud/fog environment. EMEP/MSC-E Technical report 2/2001, Meteorological Synthesizing Centre – East, Moscow, Russia

Smolarkiewicz P. K. [1982] The threedimensional Crowley advecton scheme. *Monthly Weather Review,* v.110, pp.1968-1983.

Sofiev M., Maslyaev A., and Gusev A. [1996] Heavy metal model intercomparison. Methodology and results for Pb in 1990. *EMEP/MSC-E Report 2/96*, Meteorological Synthesizing Centre – East, Moscow, Russia.

Travnikov O. [2000] Uncertainty analysis of heavy metals long-range transport modelling. EMEP/MSC-E Technical note 9/2000, July, 2000.